Impurity Transport Studies in ASDEX by Means of Neon-seeded Pellets

Kurt Behringer and Klaus Büchl

IPP III/137
IPP 1/246

August 1988

MAX-PLANCK-INSTITUT FÜR PLASMAPHYSIK

8046 GARCHING BEI MÜNCHEN

MAX-PLANCK-INSTITUT FÜR PLASMAPHYSIK

GARCHING BEI MÜNCHEN

Impurity Transport Studies in ASDEX by Means of Neon-seeded Pellets

Kurt Behringer and Klaus Büchl

IPP III/137
IPP 1/246

August 1988

Die nachstehende Arbeit wurde im Rahmen des Vertrages zwischen dem Max-Planck-Institut für Plasmaphysik und der Europäischen Atomgemeinschaft über die Zusammenarbeit auf dem Gebiete der Plasmaphysik durchgeführt.

IMPURITY TRANSPORT STUDIES IN ASDEX BY MEANS OF NEON-SEEDED PELLETS

K. Behringer and K. Büchl

Max-Planck Institut für Plasmaphysik, D-8046 Garching, FRG
EURATOM Association

Abstract

Neon-seeded deuterium pellets with a content of 1 % neon have been successfully produced and injected into ASDEX divertor discharges. The behaviour of the deposited neon ions has been studied by VUV spectroscopy using a special version of the ASDEX/JET impurity transport code for interpretation. The neutral neon source has been modelled to resemble theoretical ablation curves. Estimates of time scales for ionisation and toroidal spreading of neon ions show that toroidal symmetry is established before ionisation to NeX, while the NeVIII burn-through must be treated with caution in a 1-d model. Some ionisation and recombination rate coefficients have been verified experimentally by investigation of the time delays between pellet entry and maximum intensities, and of the low remaining level of NeVIII radiation after its ionisation peak. The anomalous neon diffusion coefficient has been derived from the final decay of the NeX line intensity, which was observed to be exponential down to the 5 % level. Below, recycling via the divertor chambers became important. A value $D \approx 0.4\ m^2/s$ was found if an associated drift velocity $v_D = -2 \cdot D \cdot r/a^2$ was assumed, which is in good a agreement with the results of other transport studies of ASDEX OH-plasmas. No apparent dependence of the diffusion coefficient on electron density was observed.

1. Introduction

Impurity transport in tokamak plasmas has often been studied by injection of test impurities and investigation of the subsequent decay of different spectral line intensities. An obvious condition for this method is a small recycling coefficient for the element in question. Traditionally, metal test impurities have been injected by laser ablation from thin films [1], producing relatively high energy (1 - 3 eV) neutral impurity atoms. Silane injection from a gas valve has been used for the same purpose [2], in that case, however, producing low energy thermal neutrals (see e.g. [3, 4] for an overview of impurity transport results). Neon puffing is normally little suited for such experiments, since the neon recycling coefficient is close to one. The ASDEX divertor experiment represents a special case in this context, because, in ASDEX, ions in the scrape-off region are swept into the divertor chambers, where they recycle at the neutraliser plates and are prevented from reentering the plasma chamber by the small effective conductance of the divertor slits (a discussion of impurity retainment in the ASDEX divertor can be found in [5]). Therefore, a partial pressure of neon builds up, and, eventually, the majority of the recycling impurity ions is found in the divertor chambers with only a small flux leaking back into the main plasma. A similar behaviour might occur in open divertor configurations with impurity retainment, as observed in Doublet III [6].

However, even in ASDEX, recycling plays an important role, when puffing neon from a gas valve [5], because the time constant for pressure build-up in the divertor chambers is similar to the transport time of ions from the edge into the interior of the plasma, where they are normally investigated by means of VUV spectroscopy. In the present paper, a new method of neon injection is used, namely, injection deep into the plasma by means of a neon-seeded deuterium pellet. In that case, highly ionised neon ions can be investigated almost instantaneously before the above processes take place, and the subsequent transport of neon ions into the divertor chambers results in a very small effective recycling coefficient. Furthermore, some interesting information on atomic rate coefficients can be obtained.

In the following, some technical details will be presented concerning the production of neon-seeded pellets from respective gas mixtures. After this technical part, spectroscopic investigations will be described dealing with the behaviour of different ionisation stages of neon deposited in the ASDEX plasma by means of a neon-seeded deuterium pellet.

From the latter investigations, values have been derived for neon transport coefficients in the target plasma.

2. Production of Neon-Seeded Pellets

A single shot light gas gun was used for production and acceleration of neon-seeded deuterium pellets. A detailed description of the injector itself is given in [7] . The injector operates by extrusion of solid material from a storage volume into the gun lock. In the usual case of deuterium, the first step is condensation of deuterium gas in the cryostat. As soon as the regulation valve is opened, the gas is supplied through a feedline from a bottle at room temperature. The condensation process itself is controlled by two parameters, ie. the flow velocity of the deuterium gas and the temperature of the cryostat, which is determined by a preset flow of liquid helium and electrical heating as required. There is an upper limit for the gas flow, because the supplied enthalpy must not exceed the available cooling power of the cryostat or condensation is not possible. Too low temperatures lead to uneven freezing at the walls and to inhomogeneous solid D_2. Furthermore, below a certain temperature, the supplied gas condenses already in the feedline thus blocking the gas flow into the cryostat. By temperature-controlled extrusion and subsequent cutting with a revolving stainless-steel cone, cylindrical pellets of diameter 1 mm and length 1 mm were inserted into the injector barrel. The pellets were accellerated by hydrogen gas of pressure 1 – 4 MPa.

In the case of neon-seeded pellets, the usual pellet gas (deuterium or hydrogen) was replaced by a mixture of deuterium and neon. The atom concentration of neon was varied between 0.5 % and 2 %. Because of the difference in tripelpoints, ie. 18.7 K for D_2 and 24.6 K for Ne, de-mixing of the two gases during the freezing process had to be expected. Futhermore, there was the increased danger of blocking the feedline by frozen neon. These problems have been successfully overcome by careful choice and control of gas flow and temperature in the cryostat.

The solid $Ne - D_2$ mixture produced in this way can be handled in the gun as usual, because its mechanical and thermal properties are only slightly different from pure solid deuterium. During acceleration with hydrogen gas, the pellets evaporate partially due to friction at the wall and heat transfer from the propellant. Therefore, the final dimensions of the pellets after leaving the barrel were determined from flash photography. The total

atom content was calculated from the photographs with an error of about ±20%. The velocity of the pellets was determined from photo-diode signals for each shot. It ranged from 400 m/s to 1000 m/s. The lower limit is given by the force necessary to break the pellet from the wall in the gun lock.

The composition of the pellets was investigated in a series of test shots as a function of the $Ne - D_2$ mixture. The neon-seeded pellets were injected into a vacuum chamber, and, after evaporation, the neon content was measured by a mass spectrometer. For a gas mixture of 1 % neon and 99 % deuterium, the measured fraction of neon in the pellet varied between 0.75 % and 1.2 % (±20%).

3. Spectroscopic Investigations

3.1 Experiment

Neon-seeded pellets were injected into ASDEX deuterium discharges with ohmic heating during the flat-top phase of the respective pulses. The pellets were injected horizontally in the midplane of the torus. The ablation trace of each pellet was photographed by a still-camera with an integration time of 100 ms. From these photographs, the penetration depth was determined with an accuracy of ±1 cm. The length of the pellet path in the plasma varied between 20 cm and 30 cm, depending on plasma conditions, pellet mass and velocity.

In all cases discussed here, ASDEX was operated in double-null configuration with plasma currents between 340 and 370 kA. Electron densities n_e, measured by a four channel HCN interferometer and Thomson scattering, ranged from about $3 \cdot 10^{19}$ to $5 \cdot 10^{19}$ m^{-3} on axis before pellet injection and increased by some 20 % as a consequence of the pellets. Electron temperatures T_e were obtained from electron cyclotron emission and Thomson scattering. For higher densities, they were about 700 eV before the pellets and dropped to $\approx$ 500 eV after pellet injection. As an example, time traces of plasma current I_p and line average electron density $\bar{n}_e$ are shown in Fig. 1a for ASDEX pulse #6443. A pellet was injected at $t \approx 1.4$ s in this pulse, leading to an increase in $\bar{n}_e$ and a decrease in electron temperature everywhere in the plasma, as demonstrated in Fig. 1b on an expanded time scale. The cooling of the bulk plasma by the pellet ablation process has been investigated by Campbell and Eberhagen [8] for the lower density pulses referred

to in this paper. Details concerning ASDEX operation and general plasma diagnostics can be found in [9] .

The main spectroscopic diagnostics during these experiments were D_α measurements and VUV spectroscopy. A D_α filter-PIN-photodiode combination viewed the pellet ablation process through the plasma with a few μs time response. The respective signals were recorded by a storage oscilloscope. Several D_α sightlines perpendicular to the pellet path recorded the pellet arrival time at different radial locations, thus allowing a calculation of its velocity in the plasma. The 2s-2p transition in Li-like neon, NeVIII, at 77.04 nm was monitored by a 1 m McPherson normal-incidence monochromator. This signal was also recorded by the oscilloscope and, simultaneously, by the ASDEX data acquisition system, in the latter case, however, only with 0.2 ms sampling time. The normal-incidence spectrometer was about 70° away in toroidal angle from the position of the pellet injector. The resonance lines of H- and He-like neon were recorded by a crystal spectrometer almost 180° away from the pellet injector. Only the H-like 1s-2p transition of NeX at 1.213 nm will be refered to in this paper. It was recorded digitally with 2 ms sampling rate. Examples of these spectroscopic signals are shown in Figs. 2 and 3.

The upper trace of Fig. 2 shows a time history of the recorded D_α intensity during pellet injection with its typical slow rise and fast decrease as the pellet is completely ablated. From the duration of this signal, about 300 μs in the case of Fig. 2, and the measured pellet speed of $\approx$ 800 m/s, a penetration depth of 24 cm is calculated, ie. the pellet penetrates to a minor radius $r_{ab} \approx 16\ cm$. A more precise analysis for pulse #6443 yields $r_{ab} = 14\ cm$ in agreement with the photograph of the ablation trace. The pellet velocity itself is derived from light pulses from different radial locations (lowest trace in Fig. 2) resulting in the same value as measured outside the torus before pellet entry into the plasma. The intensity of the NeVIII line follows D_α with some time delay, peaks shortly after the pellet is completely ablated and then decays due to ionisation into higher charge states of neon. Figure 3 shows the time histories of NeVIII and NeX on a longer time scale. The NeX line intensity reaches its maximum considerably later than NeVIII, ie. about 10 ms after pellet injection. Then, there is a first, steep decrease due to further ionisation into fully stripped neon. Subsequently, the NeX line intensity, as well as those of all other ionisation stages, decreases slowly on the impurity transport time scale. This latter phase has been the object of several impurity transport studies in ASDEX.

3.2 Time Scales of Ionisation and Toroidal Symmetry

The ablation of pellet material and the ionisation of deuterium atoms require energy, which must be supplied by the plasma electrons by means of heat conduction along field lines. Because of this process, a temperature gradient develops along the respective flux tube and the local electron temperature close to the pellet drops to a low value ($\approx$ 50 eV [10]), while the pellet itself is surrounded by a cold ($\approx 1-5$ eV) high density cloud of extension $\approx$ 1 cm [11] . In the vicinity of the pellet, the neon atoms will remain in low ionisation stages, ie. NeII or NeIII. Due to the local pressure build-up, the deuterium ions start to spread along field lines with their sound speed, which, in this case, is about $5 \cdot 10^4\ m/s$. The neon ions will spread with a similar velocity due to friction with the majority deuterium ions. Therefore, in principle, it should be possible to detect neon ions in front of the normal incidence spectrometer about 40 μs after their ablation. Ionisation to higher charge states takes place after some degree of toroidal temperature equilibration, once the pellet has passed, which may take a few 100 μs [10]. Using the electron temperature after pellet ablation as measured by ECE, ie. about 300 eV at half radius, a typical time delay of 50 μs is calculated for the production of NeVIII and 15 ms for NeX. The deuterium sound speed will also increase to $1.2 \cdot 10^5\ m/s$. Altogether, NeVIII photons may be expected from the normal incidence spectrometer some 300 μs after pellet entry into the plasma scrape-off, the major fraction of this delay being due to the time required for toroidal temperature equilibration. A one-dimensional analysis, assuming complete toroidal symmetry, can be done for times later than about 1 ms, ie. after more than ten revolutions of the ions around the torus. This means that the ionisation process of NeX can be safely interpreted on the basis of the available signals and a 1-d code, while some scepticisms is appropriate with respect to rise time and peak height of the NeVIII line intensity.

3.3 Code Simulation

A modified version of the ASDEX/JET impurity transport code "STRAHL" [12] has been used for a numerical simulation of the neon ion behaviour after injection. The pellet position between plasma edge and ablation radius r_{ab} was calculated in the code from the pellet speed v_0 during each time cycle, where t=0 was defined as the pellet entry into the scrape-off, and each cycle covered 10 μs of real time. The neutral source in the code was set to zero everywhere except at two meshpoints next to the radial position of the pellet.

The source was tailored in such a way as to closely resemble theoretical ablation curves by Milora and Foster [13]. The latter predict the total amount of particles dN ablated within a radius interval dr for a given pellet speed v_0 and known plasma parameters. However, they tend to over-estimate the pellet penetration. In the code, the particle production per unit volume and time is described by a neutral atom density n_0 and the ionisation rate $n_e \cdot S_0$. Multiplying by the respective volume and using $v_0 = dr/dt$ yields

$$dN/dr = 2\pi R 2\pi r \Delta r n_0 n_e S_0 / v_0, \qquad (1)$$

where S_0 is the neutral ionisation rate coefficient, R the major radius of the torus and Δr the distance between gridpoints in the code. If the neutral source extends over more than one gridpoint, the contributions according to Eq. (1) must be added. Eq. (1) represents a prescription for n_0 on the basis of a given ablation curve dN/dr. Figure 4 shows the ablation curve, programmed in this way into the code, in comparison to calculations according to [13].

Anomalous transport coefficients were adopted for the impurity ion fluxes Γ_I, ie.

$$\Gamma_I = -D(dn_I/dr + 2r \cdot n_I/a^2), \qquad (2)$$

where n_I are the impurity ion densities and a is the minor radius of the plasma. The drift velocity v_D, defined in this way, leads to moderately peaked stationary impurity ion profiles similar to that of the electrons [14]. The anomalous diffusion coefficient D was assumed to be constant and the same value for all impurity ions. In the calculations, it was adjusted as to reproduce the observed exponential decay of neon line emission during the transport phase after pellet injection.

Examples of such code calculations, using the actual radial profiles of electron density and electron temperature, will be shown in the next paragraph in comparison to the results of the spectroscopic measurements. Figure 5 illustrates at which radial positions NeVIII and NeX radiation shells are expected from the code calculation under similar conditions to the ones of this experiment (dashed lines). It also shows experimental radiation profiles, which were obtained by a pulse-to-pulse scan of normal incidence and crystal spectrometers. The measurements are well reproduced by the code calculation, if a diffusion coefficient $D \approx 0.4\ m^2/s$ is used [14]. These former results provide a sound basis for the present interpretation.

3.4 Results

The pellet ablation phase, as simulated by the code, is shown in Fig. 6, covering 600 μs of real time after pellet entry into the scrape-off and using 14 cm for the ablation radius r_{ab}. The dotted line represents the total number of neon ions deposited, which, on this time scale, remains constant after complete ablation. The solid curves are the code predictions for the time behaviour of different neon line intensities including NeVIII, assuming a drop in axis temperature from 725 eV to 550 eV after pellet injection. The measured NeVIII signal from Fig. 2 is also shown. The time of maximum emission and the subsequent decay are surprisingly well reproduced by the calculation, while the experimental NeVIII intensity appears to rise earlier than predicted. This discrepancy is certainly a consequence of toroidal expansion and poloidal asymmetries in the NeVIII density, which must exist at these early times. Therefore, no further interpretation has been attempted. A variation in ablation radius would only slightly modify the NeVIII behaviour via T_e and n_e profiles, while the transport parameters used in the code have no influence at all.

The ionisation phase of NeX takes about 10 ms of real time, ie. the NeX intensity is calculated to have its maximum value about 10 ms after pellet entry. Within the (considerable) experimental scatter, the predicted increase in NeX radiation is in agreement with the measured results shown in Fig. 3. Since the ablation process is long completed and toroidal symmetry has been established, this agreement may be taken as a confirmation (essentially) of the $NeIX - NeX$ ionisation rate coefficient used in the code. There are still no significant transport losses over this 10 ms time period, and the diffusion coefficient plays a minor role. The time behaviour is, however, somewhat sensitive to the ablation radius via the radial functions $T_e(r)$ and $n_e(r)$. In the comparison, 14 cm has again been adopted for r_{ab}.

The end of the NeX ionisation phase is a suitable time to measure the total number of neon ions in the plasma and to compare it to the number injected in the pellet, because toroidal symmetry is established and transport losses are still small. Using the absolutely calibrated intensity of the NeX signal and the code predictions for the ionisation balance and the radial neon ion profile, a value of $2 \cdot 10^{17}$ neon particles has been obtained for pulse #6443. The measured number of deuterium atoms in the pellet was $3 \cdot 10^{19}$, 1 % of which was supposed to be neon according to the gas mixture used for pellet production. Thus, only two thirds of the injected neon particles were found in the plasma. However, due

to the considerable error bars caused by a number of assumptions in the code analysis, this result is considered to be absolutely satisfactory.

The decay of the NeX intensity after the ionisation phase is studied in Fig. 7. Firstly, the burn-through to fully stripped neon causes a relatively steep decrease, which is a function of the NeX ionisation rate. For this H-like ion, the ionisation rate coefficient is well-known and therefore, the burn-through can rather be used for measuring the local electron temperature, which is, for a given T_e profile, a function of the ablation radius r_{ab}. It is obvious from Fig. 6 that the ablation radius from the photograph of the ablation trace, ie. 14 cm, leads to a satisfactory over-all agreement between calculated and experimental results. Subsequently, the NeX line intensity decreases exponentially according to the impurity diffusion coefficient and drift velocity (if these transport parameters were indeed functions of radius and ion charge, some average value would be measured). For an investigation of this time phase, Fig. 8 shows the NeX signal for a similar pulse on a semi-logarithmic scale.

As shown in Fig. 8, the measured NeX intensity decreases exponentially down to about 5 % of its peak height and then becomes rather constant. This is due to the fact that the neon ions leaving the plasma, as described before, are swept into the divertor chambers with only about 5 % leaking back into the main plasma. Ignoring the latter part of the data, the exponential decay is well explained by a diffusion coefficient $D = 0.4\ m^2/s$ and the associated drift velocity according to Eq. (2). Additional calculations for $D = 0.2\ m^2/s$ and $D = 0.8\ m^2/s$ demonstrate the sensitivity of the measurement with respect to D. The measured NeX decrease might just as well be explained by a diffusion coefficient of $0.6\ m^2/s$ and $v_D = 0$, as demonstrated in [15] by application of analytic transport models to the exponential decay phase. The impurity transport coefficients derived from the present experimental data are in good agreement with the ones from the positions and widths of neon radiation shells [14] and from the time behaviour of silicon line radiation after silane gas puffing [2]. Subsequent investigations of the ASDEX OH-plasma, employing the laser blow-off technique [16], confirmed these results. Little dependence on electron density has been observed in the experimental density range $\bar{n}_e = 3 \cdot 10^{19}$ to $5 \cdot 10^{19}\ m^{-3}$.

Finally, some information on the $NeIX$ - $NeVIII$ recombination rate coefficient α_8 can be obtained from the remaining low level of $NeVIII$ radiation after the burn-through of this ionisation stage. As can be shown by variation of this coefficient in the code, the ratio

of maximum emission to the following base-line level depends almost linearly on α_s. For a respective analysis of the experiment, the digital signals and the ones recorded by the oscilloscope have been joined together in order to obtain the true maximum emission. The measured ratios of NeVIII intensities at 20 ms and 50 ms to the peak at about 300 μs after pellet injection are about a factor two higher than the code prediction, which again, is a very satisfactory result considering the fact that toroidal symmetry is certainly not completely established at the early time point.

4. Summary

Neon-seeded pellets have been successfully produced and injected into ASDEX deuterium discharges. The behaviour of the deposited neon ions has been studied by VUV spectroscopy, and a special version of the ASDEX/JET impurity transport code has been used for the interpretation of the measured NeVIII and NeX line radiation. The neutral neon source in the code has been modelled to resemble theoretical ablation curves. Estimates of the relevant time scales for ionisation and toroidal spreading of the neon ions show that toroidal symmetry is already established when NeX ions are produced, while the NeVIII ionisation peak must be treated with caution in a 1-d model.

The observed time delays between pellet entry and maximum intensity of NeVIII and NeX line radiation are predicted correctly by the code calculation thus confirming, within the framework of the other assumptions, the respective ionisation rate coefficients used in the code. The burn-through of NeX is a function of the pellet penetration depth and the value derived from a photograph of the ablation trace has been verified in this way. The low remaining level of NeVIII radiation after its ionisation peak, which depends on the respective recombination rate coefficient, is also reasonably well described by the code calculation.

Once the ionisation balance is established, all intensities decrease with a time constant characteristic for the neon ion transport in the target plasma. This decay is observed to be exponential down to about 5 % of the maximum signal, when recycling via the divertor chambers becomes important. An anomalous diffusion coefficient $D \approx 0.4\ m^2/s$ is derived from the decay of NeX, if an associated drift velocity $v_D = -2 \cdot D \cdot r/a^2$ is assumed, $D \approx 0.6\ m^2/s$ results without the drift term. These values are in good agreement with

the results of other transport studies of ASDEX OH-plasmas. No apparent dependence of these transport coefficients on electron density has been observed.

Acknowledgements:
The authors are indebted to G. Fussmann for making available his crystal spectrometer data, and to many members of the ASDEX team for measurements of the plasma parameters used in the analysis. The authors are particularly grateful for E. Oberlander's technical assistance and operation of the pellet injector.

Figure Captions

Fig. 1: Plasma current and line average density for ASDEX pulse #6443 (a). Behaviour of $\bar{n}_e$ and T_e after pellet injection on an expanded time scale for the same pulse (b).

Fig. 2: Time histories of D_α and the 2s - 2p transition in NeVIII during the pellet ablation phase in pulse #6441. The lowest trace shows D_α light pulses from different radial locations used for calculation of the pellet velocity.

Fig. 3: Time histories of the NeVIII 2s - 2p and the NeX 1s - 2p transitions up to 100 ms after pellet injection.

Fig. 4: The number of ablated particles per radius interval dN/dr used in the code simulation in comparison to theoretical ablation curves [13].

Fig. 5: Measured radial emission shells of NeVIII, NeIX and NeX ions (solid lines) under plasma conditions similar to the present ones [14]. Respective code calculations are also shown (dashed lines).

Fig. 6: Code results for the pellet ablation phase showing the total number of neon ions in the plasma (dotted curve) and line intensities of several neon ion lines as a function of time after pellet entry. The measured NeVIII signal from Fig. 2 is also plotted (dashed line).

Fig. 7: Predicted time histories of the NeX line intensity after pellet injection as a function of the ablation radius r_{ab}. The initial, steeper decrease is due to further ionisation to fully stripped neon and therefore depends on the pellet penetration. Best agreement is found for $r_{ab} \approx 14$ cm.

Fig. 8: Semi-logarithmic plot of the NeX intensity decrease on the transport time scale. Recycling becomes important at the 5 % signal level. Calculations are shown for different diffusion coefficients and associated drift velocities. $D \approx 0.4\ m^2/s$ results from the comparison.

References:

[1] E.S. Marmar, J.L. Cecchi and S.A. Cohen, Rev. Sci. Instrum. **46** (1975) 1149.

[2] K. Behringer, G. Fussmann, W. Poschenrieder et al., Proc. 11th European Conf. on Contr. Fusion and Plasma Phys. **II**, Aachen (1983), p.467.

[2] C. DeMichelis and M. Mattioli, Rep. Prog. Phys. **47** (1984) 1233.

[4] R.C. Isler, Nucl. Fusion **24** (1984) 1599.

[5] G. Fussmann, W. Poschenrieder, K. Bernhardi et al., J. Nucl. Mater. **121** (1984) 164.

[6] M. Ali Mahdavi, J.C. DeBoo, C.L. Hsieh et al., Phys. Rev. Lett. **47** (1981) 1602.

[7] H. J. Forth, F.J. Otte, M. Gessinger, C. Andelfinger, K. Büchl and W. Riedmüller, Vakuumtechnik **30** (1981), 102

[8] D.J. Campbell and A. Eberhagen, Plasma Phys. and Contr. Fusion **26** (1984) 689

[9] M. Keilhacker and the ASDEX Team, Nucl.Fusion **25** (1985) 1045

[10] M Kaufmann, K. Lackner, L. Lengyel and W. Schneider, Nucl. Fusion **26** (1986) 171.

[11] TFR Group, Nucl. Fusion **27** 1987 1975

[12] K. Behringer, Report JET-R(87)08.

[13] S.L. Milora and C.A. Foster, IEEE Trans. Plasma. Sci. **6** (1978) 578.

[14] K. Behringer, W. Engelhardt, G. Fussmann et al., Proc. IAEA Techn. Comm. Meeting on Divertors and Impurity Control, Garching (1981), p.42.

[15] G. Fussmann, Nucl. Fusion **26** (1986) 983.

[16] G. Fussmann, J. Hofmann, G. Janeschitz et al., in print J. Nucl. Mater. (8th PSI, Jülich 1988).

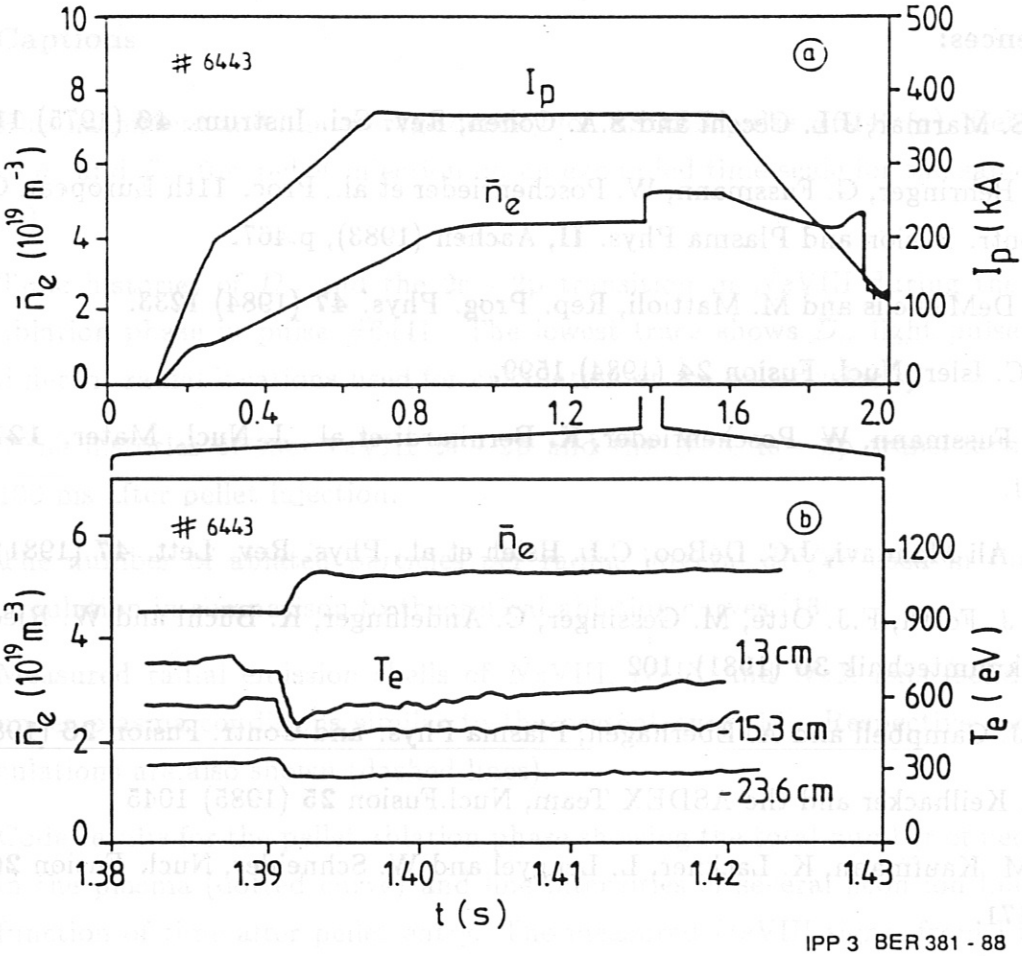

FIGURE 1

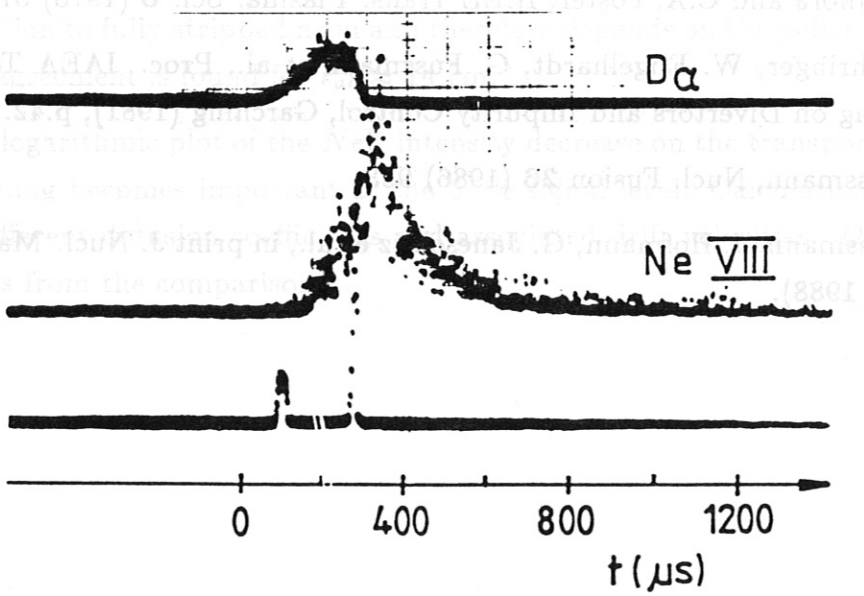

FIGURE 2

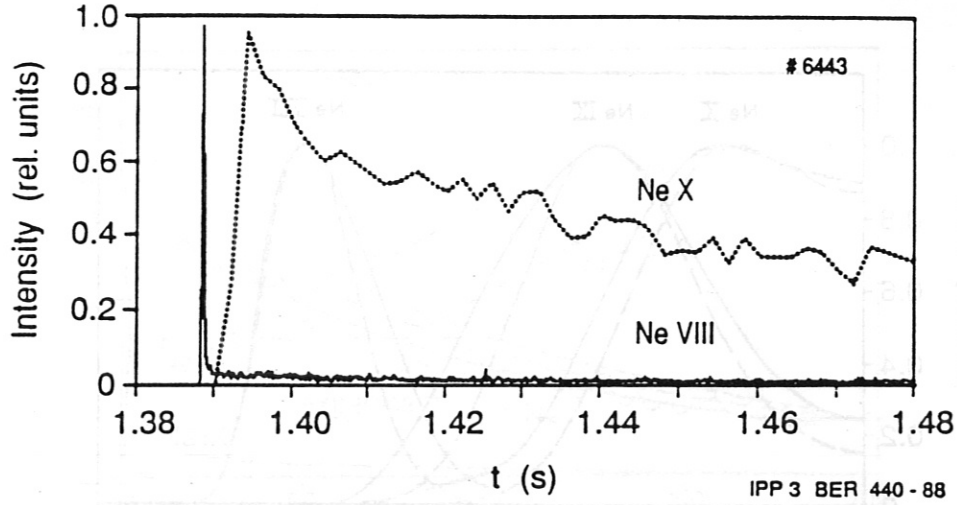

FIGURE 3

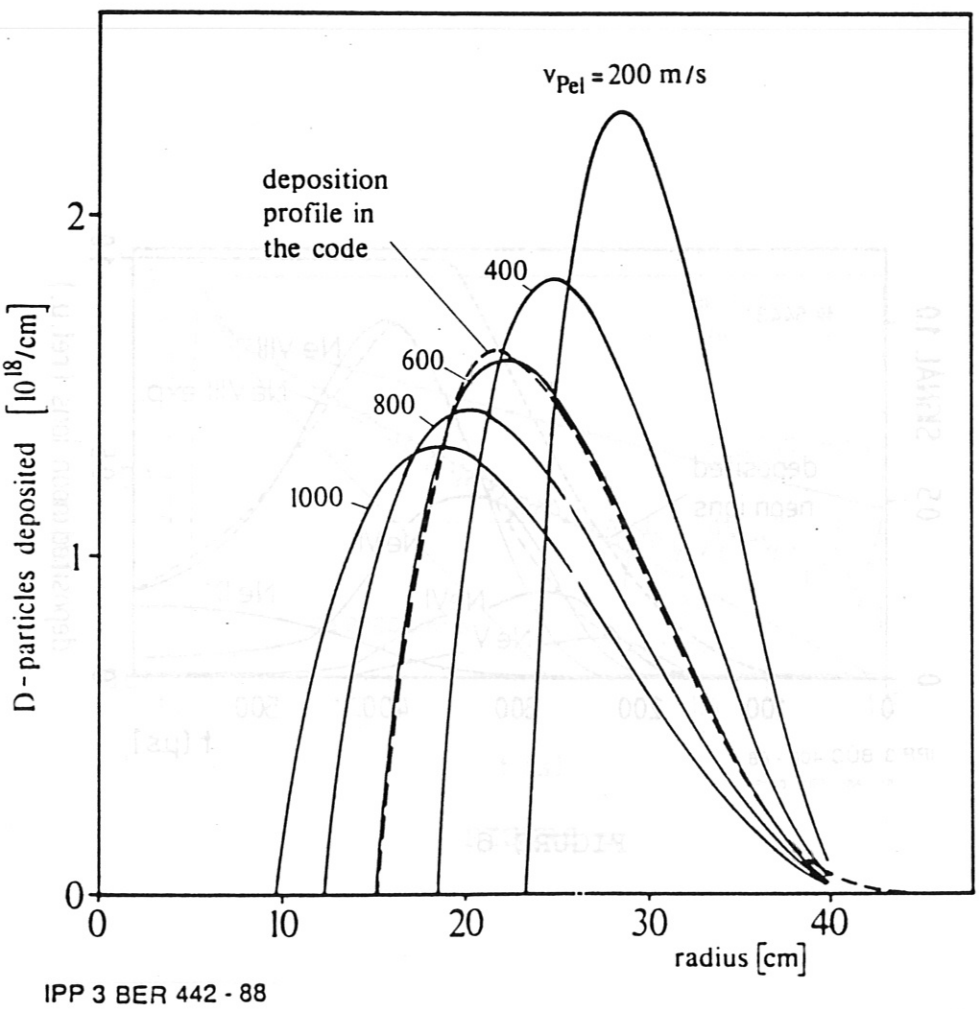

IPP 3 BER 442 - 88

FIGURE 4

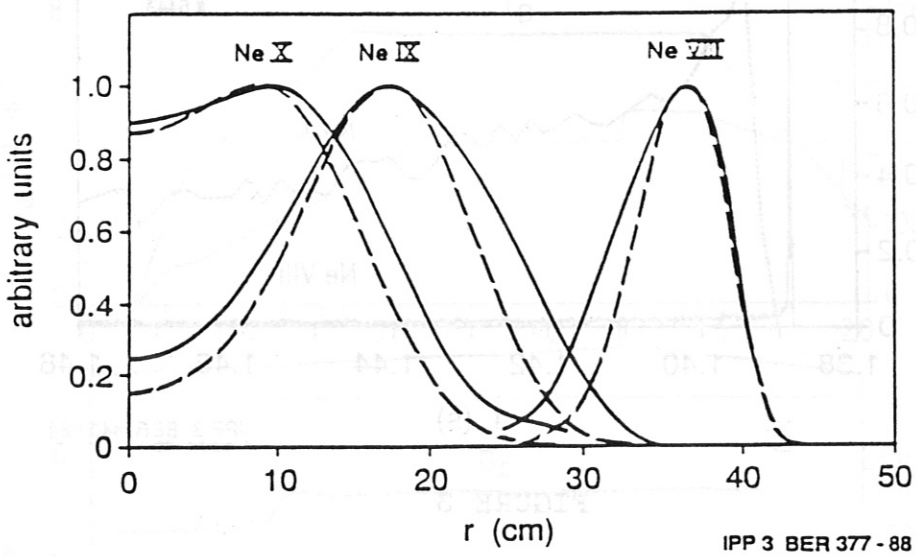

FIGURE 5

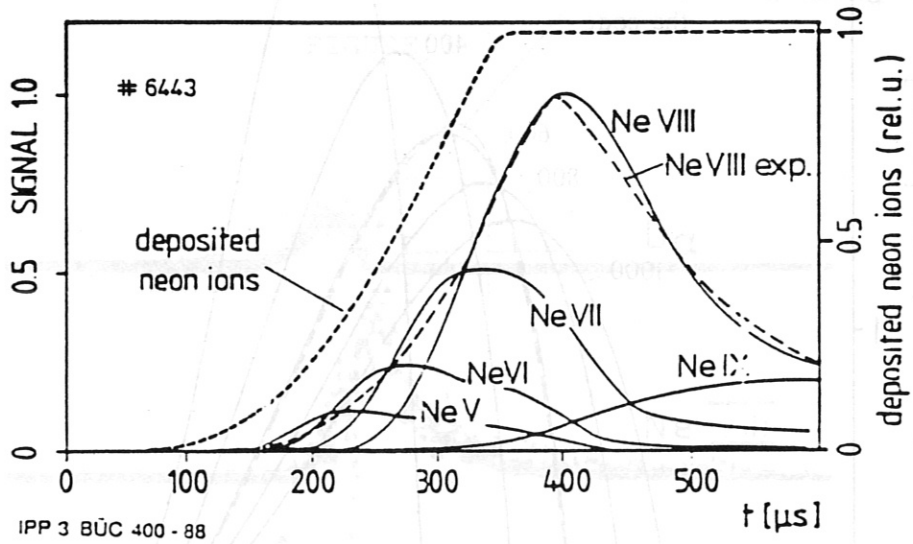

FIGURE 6

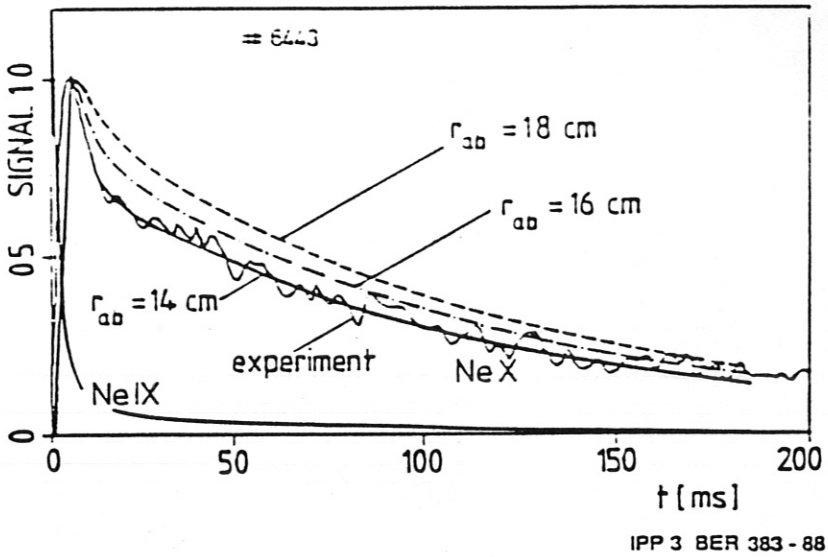

FIGURE 7

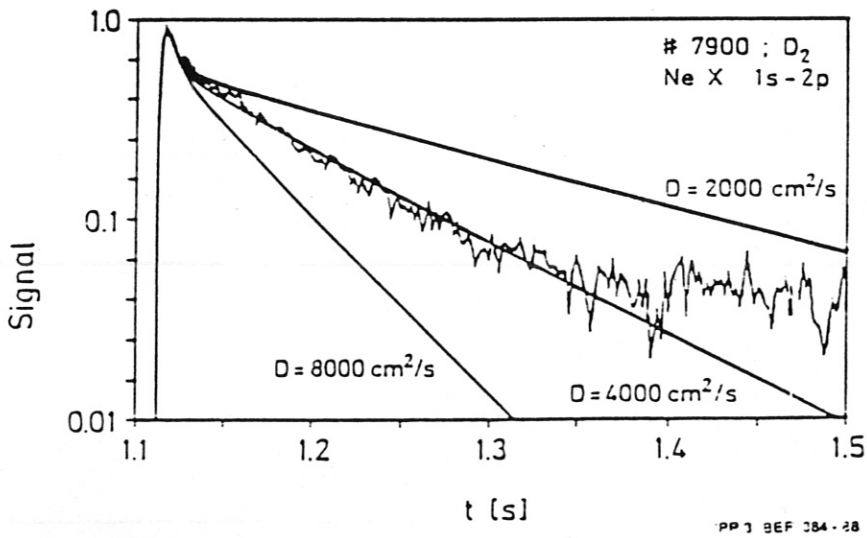

FIGURE 8